

Search for Damped Oscillating Structures from Charged Pion Electromagnetic Form Factor Data

Erik Bartoš and Stanislav Dubnička

*Institute of Physics, Slovak Academy of Sciences,
Dúbravská cesta 9, SK-84511 Bratislava, Slovak Republic*

Anna Zuzana Dubníčková

*Department of Theoretical Physics, Comenius University,
Mlynská dolina, SK-84248 Bratislava, Slovak Republic*

(Dated: March 30, 2023)

The damped oscillating structures recently revealed by a three parametric formula from the proton “effective” form factor data extracted of the measured total cross section $\sigma_{tot}^{bare}(e^+e^- \rightarrow p\bar{p})$ still seem to have an unknown origin. The conjectures of their direct manifestation of the quark-gluon structure of the proton indicate that they are not specific only of the proton and neutron, but they have to be one’s own, similar to other hadrons. Therefore, the oscillatory structures from the charged pion electromagnetic form factor timelike data, extracted of the process $e^+e^- \rightarrow \pi^+\pi^-$ are investigated by using the same procedure as in the case of the proton. The analysis shows the appearance of the oscillating structures in the description of the charged pion electromagnetic form factor timelike data by three parametric formula with a rather large value of χ^2/ndf , while the description of the data by the physically well-founded Unitary and Analytic model has not revealed any damped oscillating structures. From the obtained result on the most simple object of strong interactions, one can conclude that damped oscillating structures received from the “effective” proton form factor data are probably generated by a utilization of the improper three parametric formula which does not describe these data with sufficient precision.

Keywords: charged pion; form factors; cross sections; damped oscillations

I. INTRODUCTION

The total cross section $\sigma_{tot}^{bare}(e^+e^- \rightarrow p\bar{p})$ has been measured by two different methods, the so called scan method [1–6] and the initial state radiation (ISR) technique [7–11].

The scan method consists of taking energy scan data on the process $e^+e^- \rightarrow p\bar{p}$, whereby the c. m. energy of the e^+e^- collider is systematically changed from one energy value to another other energy value.

The ISR technique provides data on the process $e^+e^- \rightarrow p\bar{p}\gamma$ at a fixed c. m. energy value of

the e^+e^- collider at which maximal value of the luminosity is achieved, analysing events together with a photon emitted by the initial electron or positron, thus reducing the momentum transfer q^2 of the process. This method allows for the measurement of $\sigma_{tot}^{bare}(e^+e^- \rightarrow p\bar{p})$ from the threshold of the reaction $e^+e^- \rightarrow p\bar{p}$ up to the fixed c. m. energy of the e^+e^- collider.

In practical applications of both methods for obtaining experimental information on $\sigma_{tot}^{bare}(e^+e^- \rightarrow p\bar{p})$, and so also on electromagnetic (EM) form factors (FFs), it was clearly demonstrated that by means of the ISR technique more precise information has been achieved. Therefore, in this paper the data obtained by ISR technique will be preferred.

A theoretical behavior of $\sigma_{tot}^{bare}(e^+e^- \rightarrow p\bar{p})$ is described by the relation

$$\sigma_{tot}(e^+e^- \rightarrow p\bar{p}) = \frac{4\pi\alpha^2 C_p \beta_p(s)}{3s} \left[|G_M^p(s)|^2 + \frac{2m_p^2}{s} |G_E^p(s)|^2 \right], \quad (1)$$

with $\beta_p(s) = \sqrt{1 - \frac{4m_p^2}{s}}$, $\alpha=1/137$ and $C_p = \frac{\pi\alpha/\beta_p(s)}{1-\exp(-\pi\alpha/\beta_p(s))}$ to be the so-called Sommerfeld-Gamov-Sakharov Coulomb enhancement factor [12], which accounts for the EM interaction between the outgoing proton and antiproton.

The functions $G_E^p(s)$ and $G_M^p(s)$ in Equation (1) are the Sachs proton electric and proton magnetic FFs, respectively, depending on the c. m. energy squared s differently, however, at the proton-antiproton threshold they are identical as it follows from their expressions through the proton Dirac $F_1^p(s)$ and the proton Pauli $F_2^p(s)$ FFs;

$$G_E^p(s) = F_1^p(s) + \frac{s}{4m_p^2} F_2^p(s) \quad (2)$$

$$G_M^p(s) = F_1^p(s) + F_2^p(s). \quad (3)$$

As one could not determine both proton EM FFs from measured $\sigma_{tot}^{bare}(e^+e^- \rightarrow p\bar{p})$ at any value $s > 4m_p^2$ simultaneously, experimental groups in [3, 6, 8, 10, 11], with the hope of achieving more information on the proton structure, generalized the threshold identity $|G_E^p(4m_p^2)| \equiv |G_M^p(4m_p^2)|$ in Equation (1) for all higher s -values up to $+\infty$, and the data with errors obtained by means of the consequent expression

$$|G_{eff}^p(s)| = \sqrt{\frac{\sigma_{tot}^{bare}(e^+e^- \rightarrow p\bar{p})}{\frac{4\pi\alpha^2 C_p \beta_p(s)}{3s} \left(1 + \frac{2m_p^2}{s}\right)}} \quad (4)$$

have been named the proton “effective” FF data. Immediately after the publishing of the BABAR Collaboration proton “effective” FF data [8, 9], the modified form [13] of the dipole formula for nucleon EM FFs behaviors in the spacelike region

$$G_{eff}^p = \frac{A}{(1 + s/m_a^2)(1 - s/0.71 \text{ GeV}^2)^2}, \quad (5)$$

with the nucleon “magic” number 0.71 GeV^2 has been applied successfully for their description.

Here we would like to note, that the nucleon “magic” number 0.71 GeV^2 in Equation (5) has its historical origin [14] in a simultaneous description of all spacelike data on the EM FFs of the proton $G_E^p(t)$, $G_M^p(t)$ obtained from the corresponding differential cross section by means of the Rosebluth method and the spacelike neutron EM FFs $G_E^n(t)$, $G_M^n(t)$ data by only one dipole formula

$$G_E^p(t) \approx \frac{G_M^p(t)}{\mu_p} \approx \frac{G_M^n(t)}{\mu_n} \approx -\frac{4m_n^2}{t} \frac{G_E^n(t)}{\mu_n} \approx \frac{1}{(1 - \frac{t}{0.71 \text{ GeV}^2})^2} \quad (6)$$

where “ t ” is the momentum transfer squared of the elastic scattering of electrons on nucleons and magnetic moments of the proton μ_p and the neutron μ_n , respectively, which, however, is no longer valid for the following reasons.

The differential cross section of an elastic scattering of electrons on protons looks as follows

$$\frac{d\sigma}{d\Omega} = \left(\frac{d\sigma}{d\Omega} \right)_{Mott} \left\{ \frac{(G_E^p(t))^2 - \frac{t}{4m_p^2} (G_M^p(t))^2}{1 - \frac{t}{4m_p^2}} - \frac{t}{2m_p^2} (G_M^p(t))^2 \tan^2 \theta/2 \right\} \quad (7)$$

with E the electron energy and θ the electron scattering angle,

$$\left(\frac{d\sigma}{d\Omega} \right)_{Mott} = \frac{\alpha^2}{4E^2 \sin^2 \theta/2} \cdot \frac{\cos^2 \theta/2}{1 + \frac{2E}{m_p} \sin^2 \theta/2} \quad (8)$$

represents the cross section for a structureless proton. Then, the ratio $\left(\frac{d\sigma}{d\Omega} \right) / \left(\frac{d\sigma}{d\Omega} \right)_{Mott}$ when evaluated for a fixed momentum transfer squared “ $-t'$ ” yields a straight line when plotted against $\tan^2 \theta/2$. The slope of this straight line and intercept give the $G_E^p(t)$ and $G_M^p(t)$ FFs values. Such method of experimental determination of $G_E^p(t)$ indicated its dipole behaviour, but with increased “ $-t$ ” the reliability of determined $G_E^p(t)$ values acquired decreasing tendency.

Starting from 2000, the Akhiezer-Rekalo polarization method [15, 16] consisting in the simultaneous measurements of the transverse

$$P_t = \frac{h}{I_0} (-2) \sqrt{\tau(1+\tau)} G_E^N G_M^N \tan(\theta/2) \quad (9)$$

and longitudinal

$$P_l = \frac{h(E+E')}{I_0 m_N} \sqrt{\tau(1+\tau)} G_M^{N2} \tan^2(\theta/2) \quad (10)$$

components of the recoil nucleon’s polarization in the electron scattering plane of the polarization transfer $e^- N \rightarrow e^- \vec{N}$ process, with h as the electron beam helicity, I_0 as the unpolarized cross section excluding $\left(\frac{d\sigma}{d\Omega} \right)_{Mott}$ and $\tau = Q^2/4m_N^2 = -s/4m_N^2$, new more reliable data in comparison

with those obtained by means of the Rosenbluth method on the ratio $\frac{G_E^N(s)}{G_M^N(s)} = -\frac{P_t}{P_l} \frac{(E+E')}{2m_N} \tan(\theta/2)$ have been measured [17–21], which clearly demonstrate that the electric proton FF in the spacelike region has no more dipole behavior (it has a steeper fall) and it can no more be described by the nucleon “magic” number in dipole formula of Equation (6). Despite the latter, the best fit data given by Equation (5) and the value of the free parameters $A = 7.7$ and $m_a^2 = 14.8 \text{ GeV}^2$ have been subtracted from BABAR data [8, 9] on the “effective” FF with errors and in the plot of these differences with errors as a function of three momentum $p(s) = \sqrt{s(\frac{s}{4m_p^2} - 1)}$ of one of the proton or antiproton in the frame where other one is at rest, damped oscillatory structures with regularly spaced maxima and minima have been revealed [22] as presented in Figure 1.

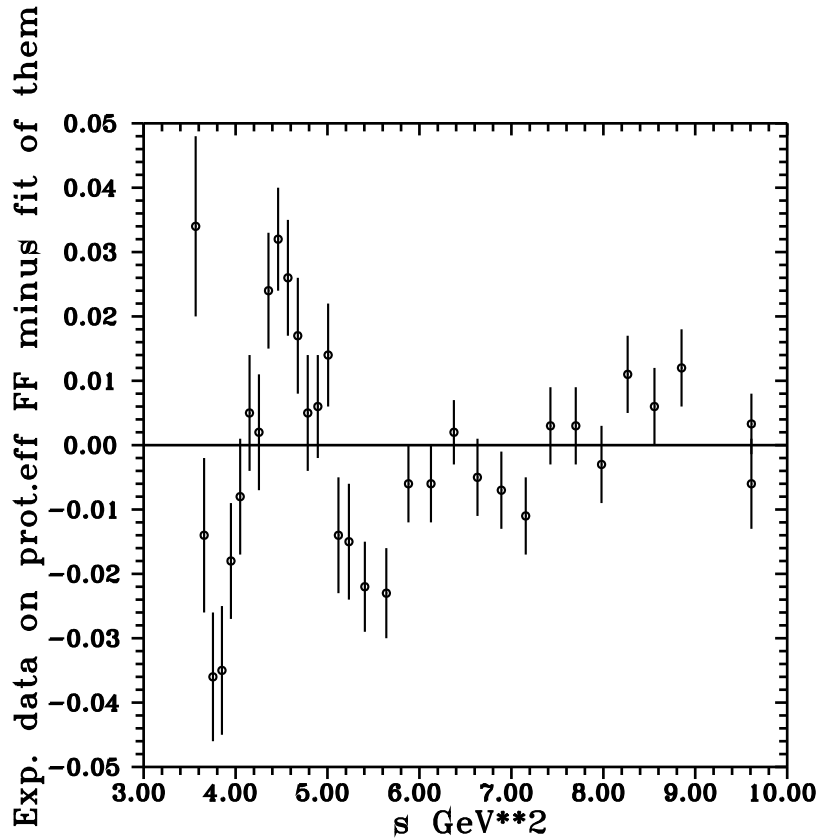


FIG. 1. Result of a subtraction of the best fit of BABAR data [8, 9] with the Formula (5) from experimental values [8, 9] with errors.

The latter oscillatory behavior, however, is seen also if results of the previous analysis are plotted simply as a function of \sqrt{s} , (see Figure 13 of [10]), consequently as a function of s too, and there is no need to plot them as a function of three momentum “ $p(s)$ ” defined by the very special reference frame.

Similar results are obtained in all other measurements of $\sigma_{tot}^{bare}(e^+e^- \rightarrow p\bar{p})$ after the year

2013 and also in the recent measurement of $\sigma_{tot}^{bare}(e^+e^- \rightarrow n\bar{n})$ [23], however, in this case with an opposite behavior.

In order to be sure of all these consequences, first we have collected all existing data on the proton “effective” FF measured until now from the papers [3, 6, 8–11] and then repeated simultaneous analysis of all of them by the Formula (5). The result with slightly different values of parameters $A = 8.9 \pm 0.3$ and $m_a^2 = 9.2 \pm 0.8 \text{ GeV}^2$ confirm the analysis of the paper [22], see Figure 2, however with $\chi^2/ndf \approx 5$ to be not acceptable from the statistical point of view declaring a good description of the experimental data. As the value of χ^2/ndf is not quoted in the paper [22], we contend that also their value is not acceptable from the statistical point of view for a good description of analysed data too. On the basis of the previous results, we arrive at a conclusion that it is likely an inaccurate description of data on the proton “effective” FF by Equation (5) is responsible for an appearance of the damped oscillatory structures from the proton “effective” FF data.

If we are not right, the origin of the damped oscillatory structures from the proton “effective” FF data [24] is still unknown.

Some conjectures exist that the damped oscillatory structures are a direct manifestation of the quark-gluon structure of the proton [25]. If so, then they can not be a specific only of the proton and neutron, and they have to be one’s own also of other hadrons.

However, only in such hadrons investigations of an existence of oscillatory structures can be carried out for which a sufficiency of reliable EM FF data exists and there is also a physically well-founded theoretical model for their perfect description.

So far, both requirements are entirely fulfilled by charged pion EM FF data and also by charged K-meson EM FF data.

In this paper with an aim of a clarification of the latter problem, damped oscillatory structures from the data on the most simple strong interactions object, the charged pion EM FF timelike data, are analysed in the framework of the model with a well-founded physical background.

Attempts to explain the damped oscillations from the proton “effective” form factor data by means of a tangible physical background approach can be found in the paper [26].

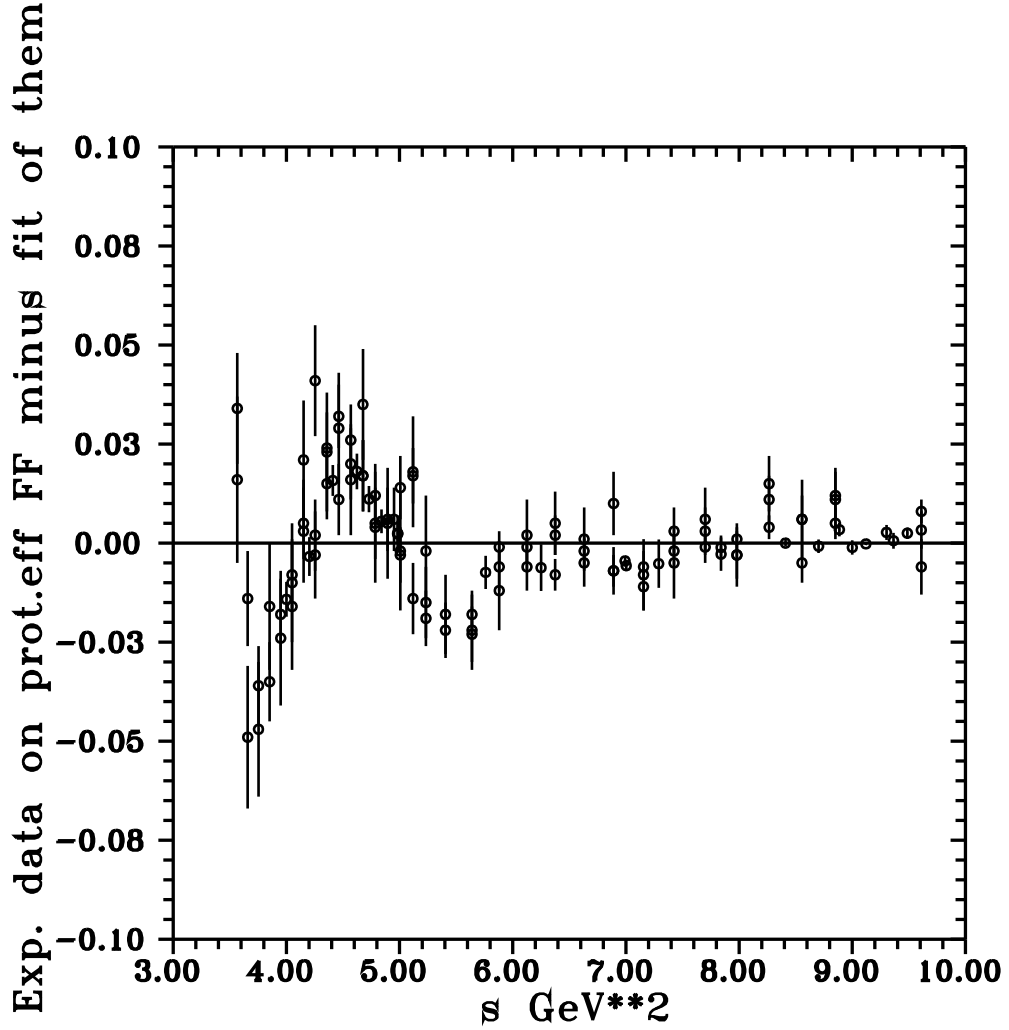


FIG. 2. Result of a subtraction of the best fit of all existing data on the proton “effective” form factor from these data with errors.

II. SEARCH FOR DAMPED OSCILLATION STRUCTURES IN THE CHARGED PION EM FF TIMELIKE DATA

The timelike data on the charged pion EM FF $F_\pi^c(s)$ with errors are hidden in the measured total cross section $\sigma_{tot}^{bare}(e^+e^- \rightarrow \pi^+\pi^-)$.

We would like to point out at once at the beginning that in the process of obtaining information on $|F_\pi^c(s)|$ from $\sigma_{tot}^{bare}(e^+e^- \rightarrow \pi^+\pi^-)$, no nonphysical demands are needed, unlike the nucleon “effective” FF data, because there is only one function $|F_\pi^c(s)|$ completely describing the measured total cross section.

However, we meet another problem here. The charged pion EM FF $F_\pi^c(s)$ represents the $\gamma\pi^+\pi^-$ vertex generated by the strong interactions and not all of $\pi^+\pi^-$ pairs in the measured total cross

section $\sigma_{tot}^{bare}(e^+e^- \rightarrow \pi^+\pi^-)$ have strong interaction origin. Some part of them appears due to electromagnetic isospin violating decay of $\omega(782) \rightarrow \pi^+\pi^-$ responsible for a deformation of the right wing of the $\rho(770)$ meson peak, well known as the ρ - ω -interference effect. Since we are investigating oscillation structures to be own of the electromagnetic FFs, one has to get rid of the electromagnetic isospin violating decay of $\omega(782) \rightarrow \pi^+\pi^-$ contribution somehow. Experimentalists are unable to isolate the electromagnetic isospin violating $\omega(782) \rightarrow \pi^+\pi^-$ decay contribution from remaining.

In three of the most precise measurements until now [27–29] of the total cross section $\sigma_{tot}^{bare}(e^+e^- \rightarrow \pi^+\pi^-(\gamma))$ with the initial state radiation (ISR) method, covering the energy range from the threshold up to 9 GeV², for elimination of the electromagnetic isospin violating decay of $\omega(782) \rightarrow \pi^+\pi^-$ contribution the following procedure will be applied.

First, the total cross section of the $e^+e^- \rightarrow \pi^+\pi^-$ process is expressed by means of the absolute value squared of the sum of $F_\pi^c(s)$ and the isospin violating $\omega(782) \rightarrow \pi^+\pi^-$ decay contribution (further denoted by $F'_\pi(s)$) in the form

$$\sigma_{tot}^{bare}(e^+e^- \rightarrow \pi^+\pi^-) = \frac{\pi\alpha^2\beta_\pi^3(s)}{3s} \left| F_\pi^c(s) + Re^{i\phi} \frac{m_\omega^2}{m_\omega^2 - s - im_\omega\Gamma_\omega} \right|^2, \quad (11)$$

where $F_\pi^c(s)$ is just the pure isovector charged pion EM FF to be expressed by the physically well founded Unitary and Analytic (U&A) model given over the Formula (3.66) from [30]

$$\begin{aligned} F_\pi^{th}[W(s)] = & \left(\frac{1 - W^2}{1 - W_N^2} \right)^2 \frac{(W - W_Z)(W_N - W_P)}{(W_N - W_Z)(W - W_P)} \\ & \times \left[\frac{(W_N - W_\rho)(W_N - W_\rho^*)(W_N - 1/W_\rho)(W_N - 1/W_\rho^*)}{(W - W_\rho)(W - W_\rho^*)(W - 1/W_\rho)(W - 1/W_\rho^*)} \left(\frac{f_{\rho\pi\pi}}{f_\rho} \right) \right. \\ & \left. + \sum_{v=\rho', \rho'', \rho'''} \frac{(W_N - W_v)(W_N - W_v^*)(W_N + W_v)(W_N + W_v^*)}{(W - W_v)(W - W_v^*)(W + W_v)(W + W_v^*)} \left(\frac{f_{v\pi\pi}}{f_v} \right) \right], \end{aligned} \quad (12)$$

which respects all well known properties of the isovector EM FF of the charged pion, similar to the analyticity in the form of two square root type of branch points approximation, first by the lowest threshold $s_0 = 4m_\pi^2$ and the second s_{in} representing contributions of all higher eventual inelastic processes effectively, therefore it is a free parameter of the model, numerically evaluated in a fitting procedure of existing data.

$$W(s) = i \frac{\sqrt{(\frac{s_{in}-s_0}{s_0})^{1/2} + (\frac{s-s_0}{s_0})^{1/2}} - \sqrt{(\frac{s_{in}-s_0}{s_0})^{1/2} - (\frac{s-s_0}{s_0})^{1/2}}}{\sqrt{(\frac{s_{in}-s_0}{s_0})^{1/2} + (\frac{s-s_0}{s_0})^{1/2}} + \sqrt{(\frac{s_{in}-s_0}{s_0})^{1/2} - (\frac{s-s_0}{s_0})^{1/2}}} \quad (13)$$

is the conformal mapping of the four sheeted Riemann surface in s variable into one W -plane,

$$W_N = W(0) = i \frac{\sqrt{(\frac{s_{in}-s_0}{s_0})^{1/2} + i} - \sqrt{(\frac{s_{in}-s_0}{s_0})^{1/2} - i}}{\sqrt{(\frac{s_{in}-s_0}{s_0})^{1/2} + i} + \sqrt{(\frac{s_{in}-s_0}{s_0})^{1/2} - i}} \quad (14)$$

is the normalization point in W-plane and

$$W_v = W(s_v) = i \frac{\sqrt{(\frac{s_{in}-s_0}{s_0})^{1/2} + (\frac{s_v-s_0}{s_0})^{1/2}} - \sqrt{(\frac{s_{in}-s_0}{s_0})^{1/2} - (\frac{s_v-s_0}{s_0})^{1/2}}}{\sqrt{(\frac{s_{in}-s_0}{s_0})^{1/2} + (\frac{s_v-s_0}{s_0})^{1/2}} + \sqrt{(\frac{s_{in}-s_0}{s_0})^{1/2} - (\frac{s_v-s_0}{s_0})^{1/2}}}. \quad (15)$$

is a position of poles corresponding to all isovector vector resonances forming the Model (12).

A normalization of the model to the electric charge leads to a reduction of the number of free coupling constant ratios ($f_{v\pi\pi}/f_v$) in Equation (12) and the isovector nature of it is in the sense that only rho-meson and its excited states, i.e., $\rho(770)$, $\rho'(1450)$, $\rho''(1700)$ [31] and also the hypothetical $\rho'''(2150)$ [32], in order to cover the energetic region of data up to 9 GeV^2 , can contribute to the FF behavior. The reality condition $F_\pi^*(s) = F_\pi(s^*)$ has an effect of an appearance always two complex conjugate rho-meson poles on unphysical sheets. The lefthand cut on the second Riemann sheet, revealed by the analytic continuation of the elastic FF unitarity condition, is approximated, in a sense of Padé, by one pole W_P and one zero W_Z , with their free positions.

Further, in Equation (11) $\phi = \arctan \frac{m_\omega \Gamma_\omega}{m_\rho^2 - m_\omega^2}$ is the $\rho - \omega$ interference phase and R is the $\rho - \omega$ interference real amplitude.

In order to recognize all optimal parameter values of the model, an analysis of existing data in [27–29] on $|F'_\pi(s)|^2$ has been carried out and the obtained results are presented numerically in Table I and graphically by the curves in Figure 3 and in detail of the $\rho - \omega$ interference effect in Figure 4.

TABLE I. Parameter values of the analysis of data in [27–29] with minimum of $\chi^2/ndf = 0.988$.

$s_{in} = 1.2730 \pm 0.0130 \text{ (GeV}^2\text{)}$	$m_\rho = 0.7620 \pm 0.0080 \text{ (GeV)}$	$\Gamma_\rho = 0.1442 \pm 0.0014 \text{ (GeV)}$
$(f_{\rho'\pi\pi}/f_{\rho'}) = -0.0706 \pm 0.0012$	$m_{\rho'} = 1.3500 \pm 0.0110 \text{ (GeV)}$	$\Gamma_{\rho'} = 0.3320 \pm 0.0033 \text{ (GeV)}$
$(f_{\rho''\pi\pi}/f_{\rho''}) = 0.0580 \pm 0.0010$	$m_{\rho''} = 1.7690 \pm 0.0180 \text{ (GeV)}$	$\Gamma_{\rho''} = 0.2531 \pm 0.0025 \text{ (GeV)}$
$(f_{\rho'''\pi\pi}/f_{\rho'''}) = 0.0021 \pm 0.0005$	$m_{\rho'''} = 2.2470 \pm 0.0110 \text{ (GeV)}$	$\Gamma_{\rho'''} = 0.0700 \pm 0.0007 \text{ (GeV)}$
$R = 0.0113 \pm 0.0002$	$W_Z = 0.2845 \pm 0.0033$	$W_P = 0.3830 \pm 0.0060$

Now, in order to obtain the values of the pure isovector charged pion EM FF timelike data, the absolute value squared relation in Equation (11) is expressed as a product of the complex and the complex conjugate terms

$$|F_\pi^c(s) + Re^{i\phi} \frac{m_\omega^2}{m_\omega^2 - s - im_\omega \Gamma_\omega}|^2 = \{F_\pi^c(s) + Re^{i\phi} \frac{m_\omega^2}{m_\omega^2 - s - im_\omega \Gamma_\omega}\} \cdot \{F_\pi^{c*}(s) + Re^{-i\phi} \frac{m_\omega^2}{m_\omega^2 - s + im_\omega \Gamma_\omega}\}, \quad (16)$$

and by using expressions $F_\pi^c(s) = |F_\pi^c(s)|e^{i\delta_\pi}$, $F_\pi^{c*}(s) = |F_\pi^c(s)|e^{-i\delta_\pi}$, also the identity of the pion EM FF phase with the P-wave isovector $\pi\pi$ -phase shift $\delta_\pi(s) = \delta_1^1(s)$, following from the charge pion EM FF elastic unitarity condition, practically considered to be valid up to 1 GeV², the quadratic equation for the absolute value of the pure isovector charged pion EM FF $|F_\pi^c(s)|$ is found

$$|F_\pi^c(s)|^2 + |F_\pi^c(s)| \frac{2Rm_\omega^2}{(m_\omega^2 - s)^2 + m_\omega^2 \Gamma_\omega^2} [(m_\omega^2 - s) \cos(\delta_1^1 - \phi) + m_\omega \Gamma_\omega \sin(\delta_1^1 - \phi)] \\ + \frac{R^2 m_\omega^4}{(m_\omega^2 - s)^2 + m_\omega^2 \Gamma_\omega^2} - \frac{3s}{\pi \alpha^2 \beta_\pi^3(s)} \sigma_{tot}^{bare}(e^+ e^- \rightarrow \pi^+ \pi^-) = 0. \quad (17)$$

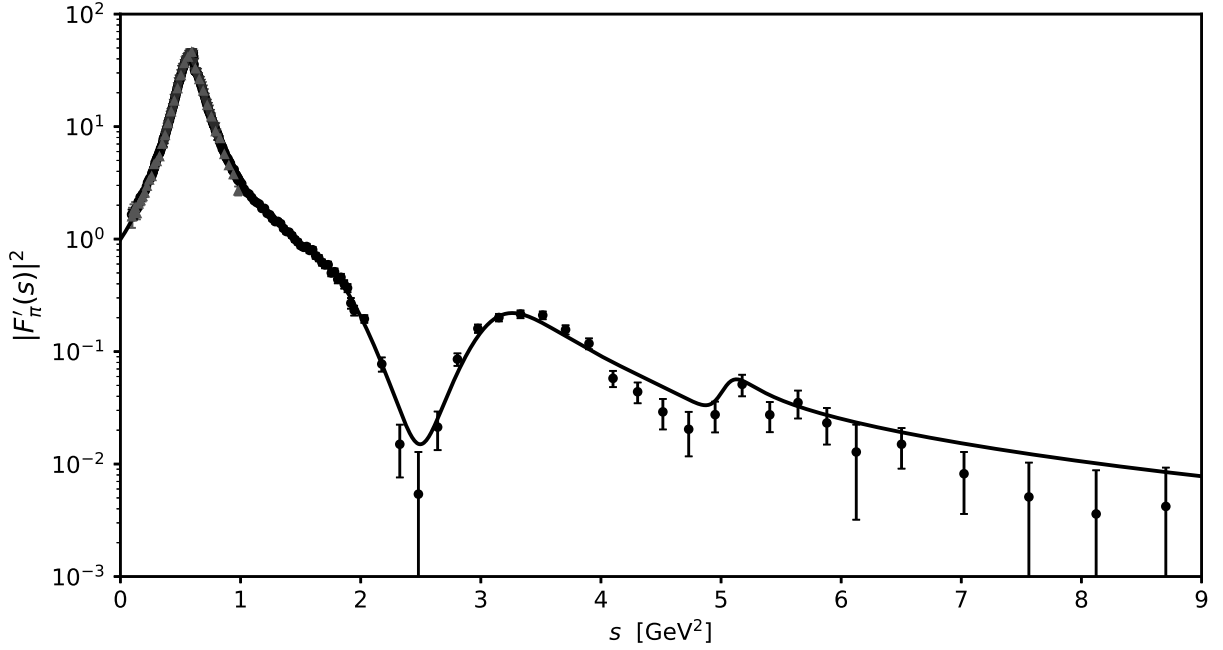


FIG. 3. Optimal description of $|F'_\pi(s)|^2$ data from [27–29] in the energy range from the threshold up to 9 GeV².

Its solution gives the relation

$$|F_\pi^c(s)| = - \frac{Rm_\omega^2}{(m_\omega^2 - s)^2 + m_\omega^2 \Gamma_\omega^2} [(m_\omega^2 - s) \cos(\delta_1^1 - \phi) + m_\omega \Gamma_\omega \sin(\delta_1^1 - \phi)] \\ \pm \left\{ \frac{R^2 m_\omega^4}{[(m_\omega^2 - s)^2 + m_\omega^2 \Gamma_\omega^2]^2} [(m_\omega^2 - s) \cos(\delta_1^1 - \phi) + m_\omega \Gamma_\omega \sin(\delta_1^1 - \phi)]^2 \right. \\ \left. - \frac{R^2 m_\omega^4}{(m_\omega^2 - s)^2 + m_\omega^2 \Gamma_\omega^2} + \frac{3s}{\pi \alpha^2 \beta_\pi^3(s)} \sigma_{tot}^{bare}(e^+ e^- \rightarrow \pi^+ \pi^-) \right\}^{1/2} \quad (18)$$

in which a physical solution is given by the “+” sign of the second term.

Then, by means of Equation (18) with the “+” sign, the most accurate up-to-now $\delta_1^1(s)$ data [33] described by the most model independent parametrization [34] with $q = [(s - 4m_\pi^2)/4]^{1/2}$, numerical values of parameters of Table I and $\sigma_{tot}^{bare}(e^+ e^- \rightarrow \pi^+ \pi^-)$ as measured in [27], the data

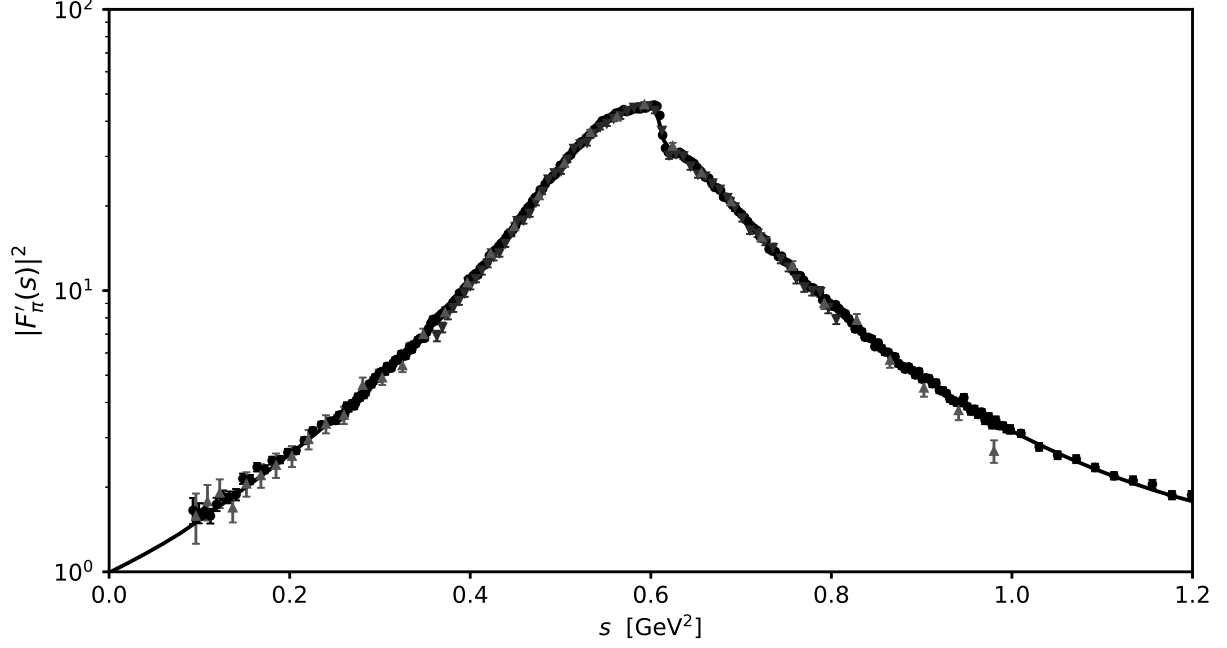


FIG. 4. Optimal description of $|F'_\pi(s)|^2$ data from [27–29] in the region of the $\rho - \omega$ -interference effect.

on the absolute value $|F_\pi^c(s)|$ of the pure isovector EM FF of the charged pion with errors are evaluated in Table II.

TABLE II: The values of $|F_\pi^c(s)|$ with errors from measurements of J.N. Lees et al. [27].

s [GeV ²]	$ F_\pi^c(s) $	s [GeV ²]	$ F_\pi^c(s) $	s [GeV ²]	$ F_\pi^c(s) $	s [GeV ²]	$ F_\pi^c(s) $
0.0930	1.2877 ± 0.0682	0.3982	3.3075 ± 0.0278	0.6384	5.6773 ± 0.0332	0.9351	2.0270 ± 0.0272
0.1056	1.2825 ± 0.0429	0.4032	3.3534 ± 0.0282	0.6448	5.5609 ± 0.0355	0.9428	2.0118 ± 0.0307
0.1190	1.3199 ± 0.0358	0.4083	3.3614 ± 0.0282	0.6512	5.4027 ± 0.0306	0.9506	1.9786 ± 0.0233
0.1332	1.3583 ± 0.0328	0.4134	3.4846 ± 0.0292	0.6577	5.2312 ± 0.0342	0.9584	1.9563 ± 0.0286
0.1482	1.4659 ± 0.0309	0.4186	3.5426 ± 0.0289	0.6642	5.1332 ± 0.0335	0.9663	1.9340 ± 0.0250
0.1640	1.5359 ± 0.0266	0.4238	3.6764 ± 0.0266	0.6708	4.9312 ± 0.0304	0.9742	1.8966 ± 0.0279
0.1806	1.5775 ± 0.0258	0.4290	3.7338 ± 0.0292	0.6773	4.8596 ± 0.0331	0.9821	1.8682 ± 0.0310
0.1980	1.6306 ± 0.0244	0.4343	3.8258 ± 0.0295	0.6839	4.7191 ± 0.0322	0.9900	1.8280 ± 0.0253
0.2162	1.7123 ± 0.0232	0.4396	3.9133 ± 0.0283	0.6906	4.5615 ± 0.0322	0.9980	1.8009 ± 0.0314
0.2352	1.8263 ± 0.0235	0.4449	3.9924 ± 0.0271	0.6972	4.4369 ± 0.0315	1.0302	1.6764 ± 0.0263
0.2510	1.8588 ± 0.0271	0.4502	4.1074 ± 0.0293	0.7039	4.3270 ± 0.0284	1.0712	1.5936 ± 0.0257
0.2550	1.8997 ± 0.0243	0.4556	4.2332 ± 0.0306	0.7106	4.1883 ± 0.0319	1.1130	1.4881 ± 0.0225
0.2591	1.9009 ± 0.0288	0.4610	4.3613 ± 0.0294	0.7174	4.1039 ± 0.0318	1.1556	1.4378 ± 0.0252
0.2632	1.9705 ± 0.0300	0.4665	4.4600 ± 0.0308	0.7242	3.9646 ± 0.0298	1.1990	1.3746 ± 0.0230

TABLE II: continued from previous page

0.2673	1.9726 ± 0.0239	0.4720	4.6090 ± 0.0285	0.7310	3.7943 ± 0.0308	1.2432	1.2880 ± 0.0247
0.2714	1.9720 ± 0.0264	0.4775	4.7514 ± 0.0320	0.7379	3.7528 ± 0.0274	1.2882	1.1999 ± 0.0228
0.2756	2.0446 ± 0.0304	0.4830	4.8630 ± 0.0289	0.7448	3.6812 ± 0.0309	1.3340	1.1756 ± 0.0247
0.2798	2.0663 ± 0.0241	0.4886	4.9630 ± 0.0312	0.7517	3.5788 ± 0.0265	1.3806	1.0842 ± 0.0227
0.2841	2.0875 ± 0.0300	0.4942	5.0519 ± 0.0326	0.7586	3.4504 ± 0.0308	1.4280	1.0412 ± 0.0242
0.2884	2.1566 ± 0.0243	0.4998	5.2457 ± 0.0329	0.7656	3.3948 ± 0.0265	1.4762	0.9737 ± 0.0249
0.2927	2.1858 ± 0.0298	0.5055	5.3471 ± 0.0333	0.7726	3.2740 ± 0.0308	1.5252	0.9220 ± 0.0231
0.2970	2.2061 ± 0.0283	0.5112	5.4675 ± 0.0341	0.7797	3.2273 ± 0.0307	1.5750	0.8929 ± 0.0239
0.3014	2.2659 ± 0.0253	0.5170	5.6229 ± 0.0318	0.7868	3.1704 ± 0.0263	1.6256	0.8460 ± 0.0255
0.3058	2.2700 ± 0.0296	0.5227	5.7551 ± 0.0351	0.7939	3.0846 ± 0.0295	1.6770	0.7899 ± 0.0250
0.3102	2.3078 ± 0.0301	0.5285	5.8519 ± 0.0313	0.8010	2.9917 ± 0.0275	1.7292	0.7714 ± 0.0249
0.3147	2.3458 ± 0.0284	0.5344	5.9386 ± 0.0334	0.8082	2.9634 ± 0.0256	1.7822	0.7180 ± 0.0250
0.3192	2.3847 ± 0.0298	0.5402	6.0875 ± 0.0359	0.8154	2.9001 ± 0.0308	1.8360	0.6780 ± 0.0248
0.3238	2.4373 ± 0.0291	0.5461	6.2520 ± 0.0368	0.8226	2.7916 ± 0.0253	1.8906	0.6083 ± 0.0252
0.3283	2.4188 ± 0.0301	0.5520	6.2996 ± 0.0369	0.8299	2.7271 ± 0.0287	1.9460	0.4836 ± 0.0242
0.3329	2.5142 ± 0.0300	0.5580	6.3527 ± 0.0374	0.8372	2.6327 ± 0.0278	2.1756	0.2798 ± 0.0201
0.3376	2.5335 ± 0.0303	0.5640	6.4270 ± 0.0343	0.8446	2.6144 ± 0.0311	2.4806	0.0746 ± 0.0504
0.3422	2.5808 ± 0.0276	0.5700	6.4872 ± 0.0361	0.8519	2.5705 ± 0.0300	2.8056	0.2934 ± 0.0186
0.3469	2.6007 ± 0.0291	0.5761	6.4301 ± 0.0356	0.8593	2.4773 ± 0.0305	3.1506	0.4488 ± 0.0172
0.3516	2.6623 ± 0.0247	0.5822	6.4563 ± 0.0360	0.8668	2.4332 ± 0.0299	3.5156	0.4595 ± 0.0183
0.3564	2.7621 ± 0.0295	0.5883	6.3945 ± 0.0360	0.8742	2.3619 ± 0.0294	3.9006	0.3440 ± 0.0191
0.3612	2.7882 ± 0.0263	0.5944	6.3437 ± 0.0408	0.8817	2.3077 ± 0.0260	4.3056	0.2100 ± 0.0220
0.3660	2.8463 ± 0.0252	0.6006	6.2978 ± 0.0423	0.8892	2.2963 ± 0.0283	4.7306	0.1433 ± 0.0305
0.3709	2.8903 ± 0.0285	0.6068	6.1805 ± 0.0393	0.8968	2.2847 ± 0.0275	5.1756	0.2265 ± 0.0246
0.3758	2.9375 ± 0.0224	0.6131	5.9525 ± 0.0367	0.9044	2.2257 ± 0.0297	5.6406	0.1880 ± 0.0261
0.3807	3.0037 ± 0.0296	0.6194	6.0538 ± 0.0391	0.9120	2.1731 ± 0.0295	6.1256	0.1135 ± 0.0424
0.3856	3.0602 ± 0.0277	0.6257	5.9463 ± 0.0339	0.9197	2.1173 ± 0.0257	7.0225	0.0908 ± 0.0254
0.3906	3.1212 ± 0.0273	0.6320	5.8797 ± 0.0374	0.9274	2.0884 ± 0.0241	8.1225	0.0602 ± 0.0433
0.3956	3.2098 ± 0.0265	—	—	—	—	—	—

$\sigma_{tot}^{bare}(e^+e^- \rightarrow \pi^+\pi^-)$ as measured in [28] the data on the absolute value $|F_\pi^c(s)|$ of the pure isovector EM FF of the charged pion with errors are evaluated in Table III, and $\sigma_{tot}^{bare}(e^+e^- \rightarrow \pi^+\pi^-)$ as measured in [29] the data on the absolute value $|F_\pi^c(s)|$ of the pure isovector EM FF of the charged pion with errors are evaluated in Table IV.

TABLE III: The values of $|F_\pi^c(s)|$ with errors from measurements of T. Xiao et al. [28].

s [GeV ²]	$ F_\pi^c(s) $	s [GeV ²]	$ F_\pi^c(s) $	s [GeV ²]	$ F_\pi^c(s) $	s [GeV ²]	$ F_\pi^c(s) $
0.0961	1.2579 ± 0.1274	0.2401	1.8320 ± 0.0678	0.4489	4.0967 ± 0.0645	0.7225	3.9831 ± 0.0712
0.1089	1.3352 ± 0.0964	0.2601	1.8998 ± 0.0676	0.4761	4.6435 ± 0.0666	0.7569	3.5322 ± 0.0712
0.1225	1.3827 ± 0.0809	0.2809	2.1465 ± 0.0695	0.5041	5.2939 ± 0.0657	0.7921	3.0313 ± 0.0717
0.1369	1.3011 ± 0.0739	0.3025	2.2129 ± 0.0638	0.5329	5.9774 ± 0.0666	0.8281	2.8224 ± 0.0731
0.1521	1.4347 ± 0.0712	0.3249	2.3250 ± 0.0614	0.5625	6.3216 ± 0.0681	0.8649	2.3964 ± 0.0730
0.1681	1.4848 ± 0.0713	0.3481	2.6404 ± 0.0637	0.5929	6.4618 ± 0.0715	0.9025	2.1373 ± 0.0742
0.1849	1.5489 ± 0.0772	0.3721	2.8870 ± 0.0631	0.6241	6.1518 ± 0.0733	0.9409	1.9482 ± 0.0749
0.2025	1.6065 ± 0.0683	0.3969	3.2578 ± 0.0644	0.6561	5.2718 ± 0.0702	0.9801	1.6492 ± 0.0752
0.2209	1.7209 ± 0.0685	0.4225	3.6715 ± 0.0648	0.6889	4.6328 ± 0.0705	—	—

TABLE IV: The values of $|F_\pi^c(s)|$ with errors from measurements of M. Ablikim et al. [29].

s [GeV ²]	$ F_\pi^c(s) $	s [GeV ²]	$ F_\pi^c(s) $	s [GeV ²]	$ F_\pi^c(s) $	s [GeV ²]	$ F_\pi^c(s) $
0.3630	2.6228 ± 0.0571	0.4590	4.2006 ± 0.0593	0.5663	6.3316 ± 0.0773	0.6848	4.7102 ± 0.0649
0.3691	2.7159 ± 0.0551	0.4658	4.3154 ± 0.0577	0.5738	6.4403 ± 0.0757	0.6931	4.5238 ± 0.0674
0.3752	2.8587 ± 0.0524	0.4727	4.5158 ± 0.0551	0.5814	6.4891 ± 0.0747	0.7014	4.3203 ± 0.0588
0.3813	2.9442 ± 0.0509	0.4796	4.7177 ± 0.0527	0.5891	6.4405 ± 0.0746	0.7098	4.1088 ± 0.0617
0.3875	3.0272 ± 0.0495	0.4865	4.9612 ± 0.0601	0.5968	6.3509 ± 0.0744	0.7183	4.0533 ± 0.0625
0.3938	3.1239 ± 0.0479	0.4935	5.0862 ± 0.0586	0.6045	6.0821 ± 0.0758	0.7268	3.9213 ± 0.0646
0.4001	3.2176 ± 0.0465	0.5006	5.1210 ± 0.0582	0.6123	5.9440 ± 0.0834	0.7353	3.8124 ± 0.0663
0.4064	3.3085 ± 0.0452	0.5077	5.3716 ± 0.0647	0.6202	5.9887 ± 0.0821	0.7439	3.6460 ± 0.0693
0.4128	3.4262 ± 0.0582	0.5148	5.6100 ± 0.0619	0.6281	5.8975 ± 0.0724	0.7526	3.5157 ± 0.0575
0.4193	3.5256 ± 0.0566	0.5220	5.7086 ± 0.0694	0.6360	5.7515 ± 0.0729	0.7613	3.3510 ± 0.0603
0.4258	3.6222 ± 0.0551	0.5293	5.7354 ± 0.0690	0.6440	5.4657 ± 0.0760	0.7700	3.2412 ± 0.0623
0.4323	3.6757 ± 0.0542	0.5366	5.9464 ± 0.0582	0.6521	5.2508 ± 0.0688	0.7788	3.1919 ± 0.0632
0.4389	3.8206 ± 0.0522	0.5439	6.0994 ± 0.0647	0.6602	5.1830 ± 0.0693	0.7877	3.1741 ± 0.0636
0.4456	3.9851 ± 0.0500	0.5513	6.1742 ± 0.0638	0.6683	5.0217 ± 0.0713	0.7966	2.9754 ± 0.0678
0.4523	4.1906 ± 0.0594	0.5588	6.2835 ± 0.0704	0.6765	4.8821 ± 0.0627	0.8055	2.8349 ± 0.0534

All three sets of data on the absolute value $|F_\pi^c(s)|$ of the pure isovector EM FF of the charged pion as a function of s of threshold up to 9 GeV² as given in Tables II–IV are graphically presented in Figure 5.

Afterwards these data are optimally described by a similar formula to Equation (5), however,

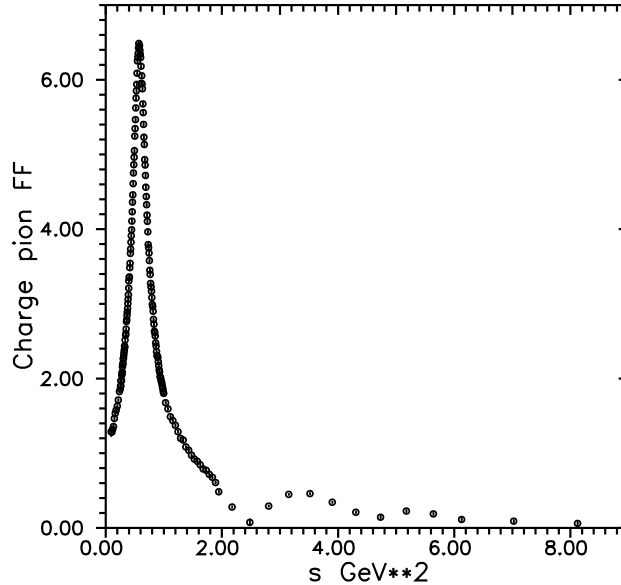


FIG. 5. Calculated values of $|F_\pi^c(s)|$ with errors from measured $\sigma_{tot}^{bare}(e^+e^- \rightarrow \pi^+\pi^-)$ in [27–29] by the Expression (18).

now the nucleon “magic” number 0.71 is substituted by the third free parameter A_3 , because one can not expect to be suitable nucleon “magic” number for optimal description of the absolute value $|F_\pi^c(s)|$ data and one has to look for the charged pion “magic” number in its place.

The best fit of the data presented in Figure 5 has been achieved with parameter values $A = 3.9888 \pm 0.0061$, $m_a^2 = 5.5647 \pm 0.1915 \text{ GeV}^2$ and the charged pion “magic” number $A_3 = -5.5647 \pm 0.1037 \text{ GeV}^2$. The result of the fit is graphically presented in Figure 6 by the dashed line.

If dashed line values are subtracted from the experimental values of $|F_\pi^c(s)|$ with errors in Tables 2–4, damped oscillating structures from charged pion electromagnetic form factor timelike data appear, as it is presented in Figure 7.

If only the data on $|F_\pi^c(s)|$ from Figure 5 just behind the distinct ρ -meson peak, starting from 1 GeV^2 up to 9 GeV^2 , are optimally described by a similar formula to Equation (5) with all three free parameters with values $A = 3.7485 \pm 0.4463$, $m_a^2 = 3.9681 \pm 0.6064 \text{ GeV}^2$, $A_3 = -2.0369 \pm 0.2613 \text{ GeV}^2$, one obtains the result graphically presented by dashed line in Figure 8, and the corresponding damped oscillating structures appear as it is presented in Figure 9.

A perfect description of the data on $|F_\pi^c(s)|$ accumulated in Tables 2–4 by Equations (12)–(15) with the numerical values of parameters of Table I is represented by the full line in Figure 10. If full line data in Figure 10 are subtracted from the data in Tables 2–4, no oscillation structures appear as it is demonstrated clearly in Figure 11.

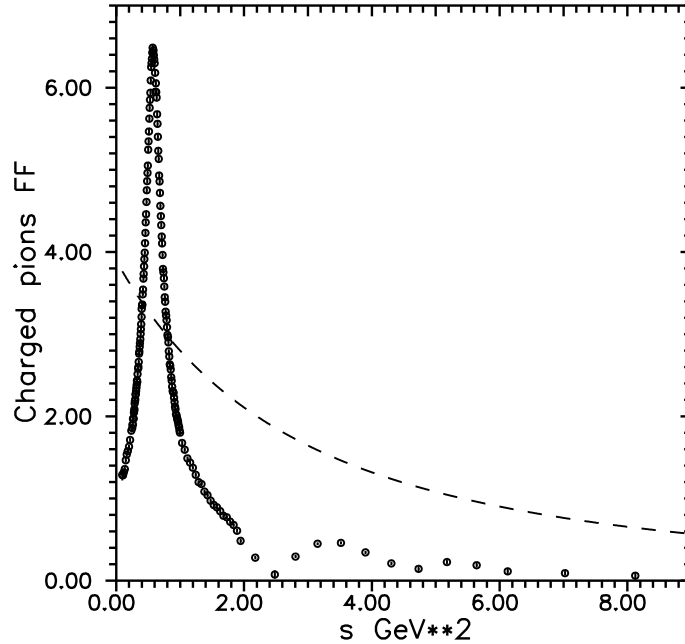


FIG. 6. Optimal description of $|F_\pi^c(s)|$ data with dashed line given by a similar formula to Equation (5), however now with the third parameter to be $A_3 = -5.5647 \pm 0.1037 \text{ GeV}^2$.

III. CONCLUSIONS AND DISCUSSIONS

The damped oscillating structures from the proton “effective” form factor data invite questions about the existence the similar oscillating structures in the case of other strong interacting particles. One can investigate them if solid data on the corresponding form factors exists together with a physically well-founded model, and by means of it the accurate description of these data is achieved. The only suitable candidates for such investigations are the charged pion and the charged kaon electromagnetic form factor data.

In this paper, the problem of the pure isovector charged pion electromagnetic form factor data by using the same procedure as in the case of the proton has been investigated. Since oscillation structures have to be concerned of the $\gamma\pi^+\pi^-$ vertex generated by the strong interactions only and the measured $\sigma_{tot}^{bare}(e^+e^- \rightarrow \pi^+\pi^-)$ contains some part of $\pi^+\pi^-$ pairs due to electromagnetic isospin violating decay of $\omega(782) \rightarrow \pi^+\pi^-$, first an elimination of a contribution of the latter into three the most precise measurements [27–29] of $\sigma_{tot}^{bare}(e^+e^- \rightarrow \pi^+\pi^-(\gamma))$ with the ISR method has been carried out. With this aim, first $\sigma_{tot}^{bare}(e^+e^- \rightarrow \pi^+\pi^-(\gamma))$ was expressed as the absolute value squared of the sum of the pure charged pion electromagnetic form factor and the $\omega(782) \rightarrow \pi^+\pi^-$ contribution expressed by the Breit-Wigner formula (see Equation (11)). Then, by exploiting the identity of the charged pion electromagnetic form factor phase with P-wave isovector $\pi\pi$ -scattering

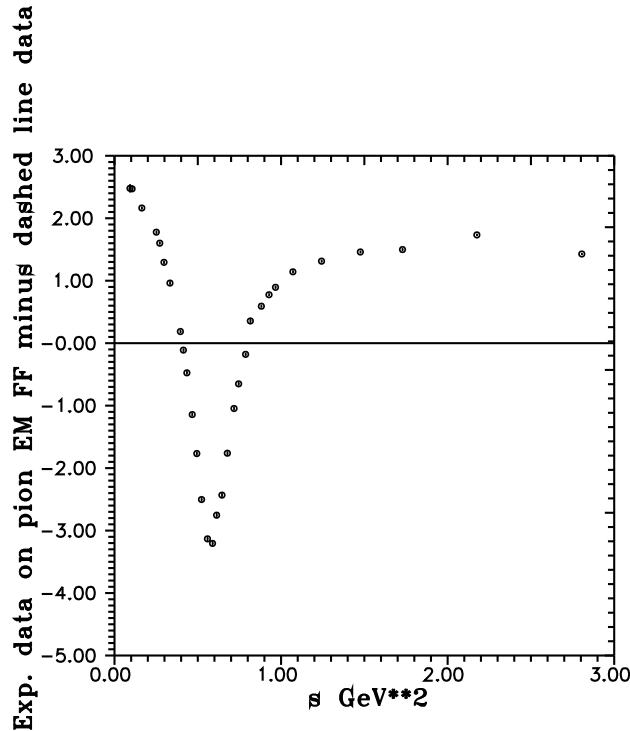


FIG. 7. Damped oscillation structures obtained by a subtraction of dashed line data in Figure 6 from exp. data on $|F_{\pi}^c(s)|$ in Tables 2–4.

phase shift and the most accurate up-to-now data of the latter, the data on the absolute value of the pure isovector electromagnetic form factor with errors have been obtained by Equation (18) in Tables II–IV. If these data are best possibly described by the adaptation to the charged pion three parametric formula (see dashed lines in Figures 6 and 8), damped oscillatory structures appear (Figures 7 and 9). If data are described by well physically founded U&A model Equations (12)–(15) (see Figure 10 with full line) no damped oscillatory structures appear as it is clearly demonstrated in Figure 11.

So, the proper usage of the physically well founded theoretical model accurately describing experimental data eliminate the effect of creating the oscillations.

Further investigations in this sense concerning the proton and also the charged K-meson are in progress.

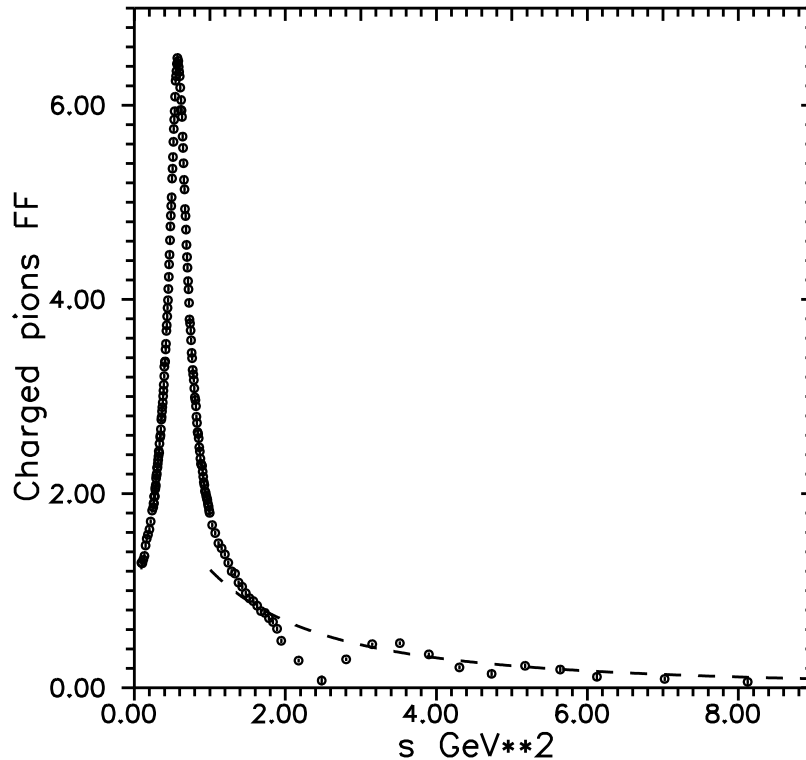


FIG. 8. Optimal description of $|F_\pi^c(s)|$ data with dashed line given by a similar formula to Equation (5), however now with the third parameter to be $A_3 = -2.0369 \pm 0.2613 \text{ GeV}^2$.

ACKNOWLEDGMENTS

This research was funded by the Slovak Grant Agency for Sciences grant number VEGA 2/0105/21.

-
- [1] Pedlar, T.K.; Cronin-Hennessy, D.; Gao, K.Y.; Gong, D.T.; Hietala, J.; Kubota, Y.; Klein, T.; Lang, B.W.; Li, S.Z.; Poling, R. ; et al. Precision measurements of the timelike electromagnetic form factors of pion, kaon, and proton. *Phys. Rev. Lett.* **2005**, *95*, 261803. <https://doi.org/10.1103/PhysRevLett.95.261803>.
 - [2] BES Collaboration; Ablikim, M.; Bai, J.Z.; Ban, Y.; Bian, J.G.; Cai, X.; Chen, H.F.; Chen, H.S.; Chen, H.X.; Chen, J.C.; et al. Measurement of the cross section for $e^+e^- \rightarrow p\bar{p}$ at center-of-mass energies from 2.0 to 3.07 GeV. *Phys. Lett. B* **2005**, *630*, 14–20. <https://doi.org/10.1016/j.physletb.2005.09.044>.
 - [3] Ablikim, M.; Achasov, M.N.; Ai, X.C.; Albayrak, O.; Albrecht, M.; Ambrose, D.J.; Amoroso, A.; An, F.F.; An, Q.; Bai, J.Z.; et al. Measurement of the $e^+e^- \rightarrow \pi^+\pi^-$ cross section between 600 and 900 MeV using initial state radiation. *Phys. Lett.* **2016**, *B753*, 629–638.

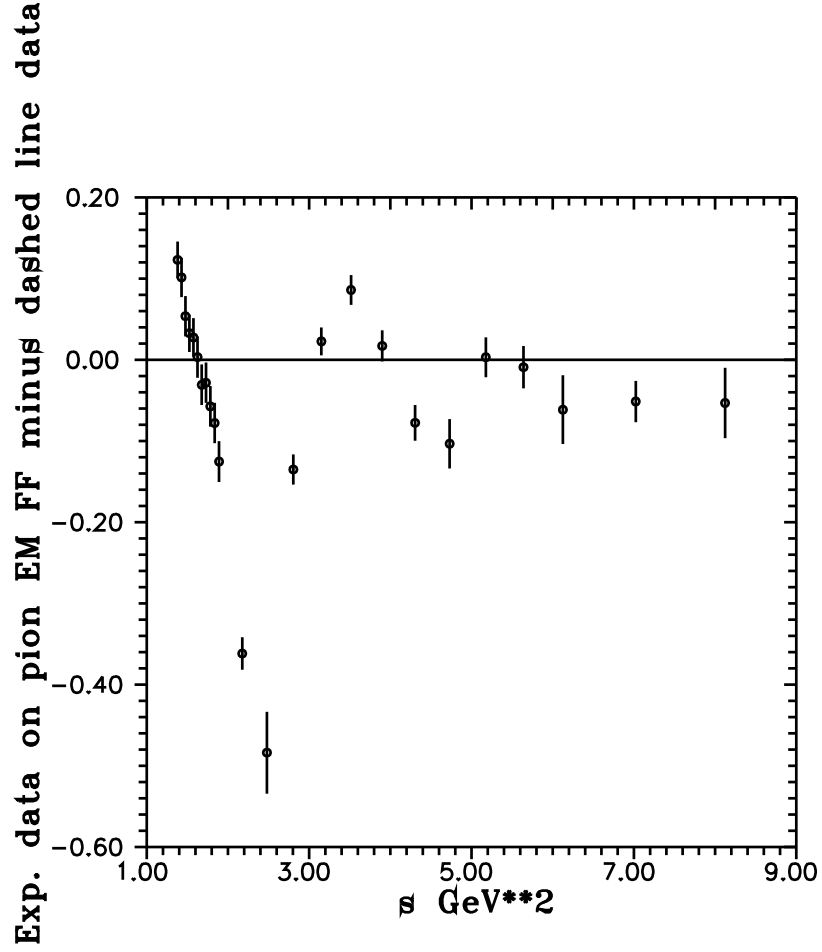


FIG. 9. Damped oscillation structures obtained by a subtraction of dashed line data in Figure 8 from exp. data on $|F_\pi^c(s)|$ in Tables 2–4.

<https://doi.org/10.1016/j.physletb.2015.11.043>.

- [4] Akhmetshin, R.R.; Amirkhanov, A.N.; Anisenkov, A.V.; Aulchenko, V.M.; Banzarov, V.S.; Bashtovoy, N.S.; Berkaev, D.E.; Bondar, A.E.; Bragin, A.V.; Eidelman, S.I.; et al. Study of the process $e^+e^- \rightarrow p\bar{p}$ in the c.m. energy range from threshold to 2 GeV with the CMD-3 detector. *Phys. Lett. B* **2016**, *759*, 634–640. <https://doi.org/10.1016/j.physletb.2016.04.048>.
- [5] Akhmetshin, R.R.; Amirkhanov, A.N.; Anisenkov, A.V.; Aulchenko, V.M.; Banzarov, V.S.; Bashtovoy, N.S.; Berkaev, D.E.; Bondar, A.E.; Bragin, A.V.; Eidelman, S.I.; et al. Observation of a fine structure in $e^+e^- \rightarrow \text{hadrons}$ production at the nucleon-antinucleon threshold. *Phys. Lett. B* **2019**, *794*, 64–68. <https://doi.org/10.1016/j.physletb.2019.05.032>.
- [6] Ablikim, M.; Achasov, M.; Adlarson, P.; Ahmed, S.; Albrecht, M.; Alekseev, M.; Amoroso, A.; An, F.; An, Q.; Anita; et al. Measurement of Proton Electromagnetic Form Factors in $e^+e^- \rightarrow p\bar{p}$ in the Energy Region 2.00–3.08 GeV. *Phys. Rev. Lett.* **2020**, *124*, 042001. <https://doi.org/10.1103/PhysRevLett.124.042001>.

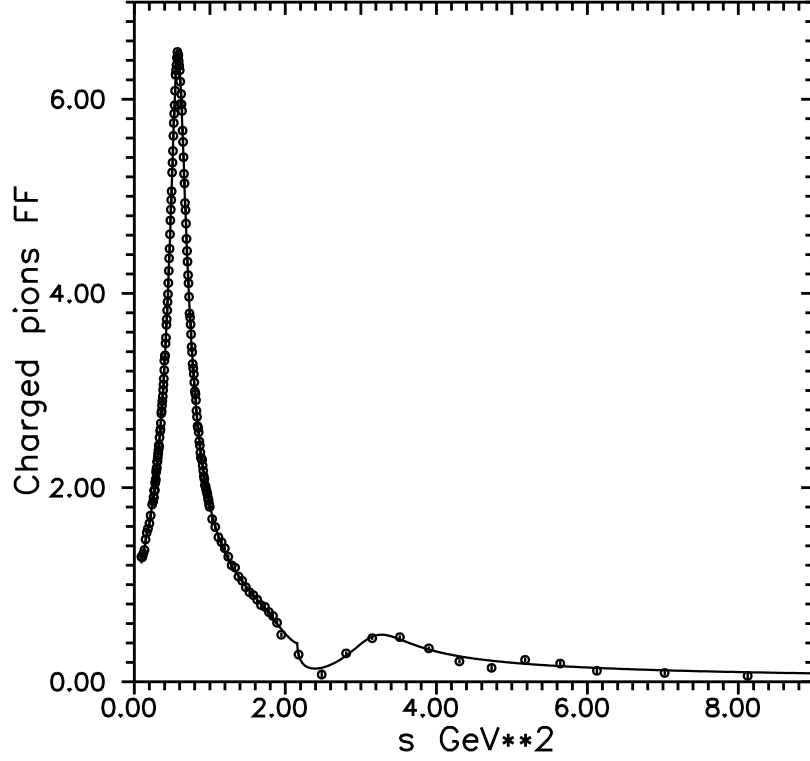


FIG. 10. Optimal description of $|F_\pi^c(s)|$ data with full line given by Equations (12)–(15) and parameters values of Table I.

- [7] Aubert, B.; Barate, R.; Boutigny, D.; Couderc, F.; Karyotakis, Y.; Lees, J.P.; Poireau, V.; Tisserand, V.; Zghiche, A.; Grauges, E.; et al. Study of $e^+e^- \rightarrow p\bar{p}$ using initial state radiation with BABAR. *Phys. Rev. D* **2006**, *73*, 012005. <https://doi.org/10.1103/PhysRevD.73.012005>.
- [8] Lees, J.P.; Poireau, V.; Tisserand, V.; Grauges, E.; Palano, A.; Eigen, G.; Stugu, B.; Brown, D.N.; Kerth, L.T.; Yu, G.; et al. Study of $e^+e^- \rightarrow p\bar{p}$ via initial-state radiation at BABAR. *Phys. Rev. D* **2013**, *87*, 092005. <https://doi.org/10.1103/PhysRevD.87.092005>.
- [9] Lees, J.P.; Poireau, V.; Tisserand, V.; Grauges, E.; Palano, A.; Eigen, G.; Stugu, B.; Brown, D.N.; Kerth, L.T.; Yu, G.; et al. Production of charged pions, kaons, and protons in e^+e^- annihilations into hadrons at $\sqrt{s} = 10.54$ GeV. *Phys. Rev. D* **2013**, *88*, 032011. <https://doi.org/10.1103/PhysRevD.88.032011>.
- [10] Ablikim, M.; Achasov, M.; Adlarson, P.; Ahmed, S.; Albrecht, M.; Alekseev, M.; Amoroso, A.; An, F.; An, Q.; Bai, Y.; et al. Study of the process $e^+e^- \rightarrow p\bar{p}$ via initial state radiation at BESIII. *Phys. Rev. D* **2019**, *99*, 092002. <https://doi.org/10.1103/PhysRevD.99.092002>.
- [11] Ablikim, M.; Achasov, M.N.; Adlarson, P.; Ahmed, S.; Albrecht, M.; Aliberti, R.; Amoroso, A.; An, M.R.; An, Q.; Bai, X.H.; et al. Measurement of proton electromagnetic form factors in the time-like region using initial state radiation at BESIII. *Phys. Lett. B* **2021**, *817*, 136328. <https://doi.org/https://doi.org/10.1016/j.physletb.2021.136328>.

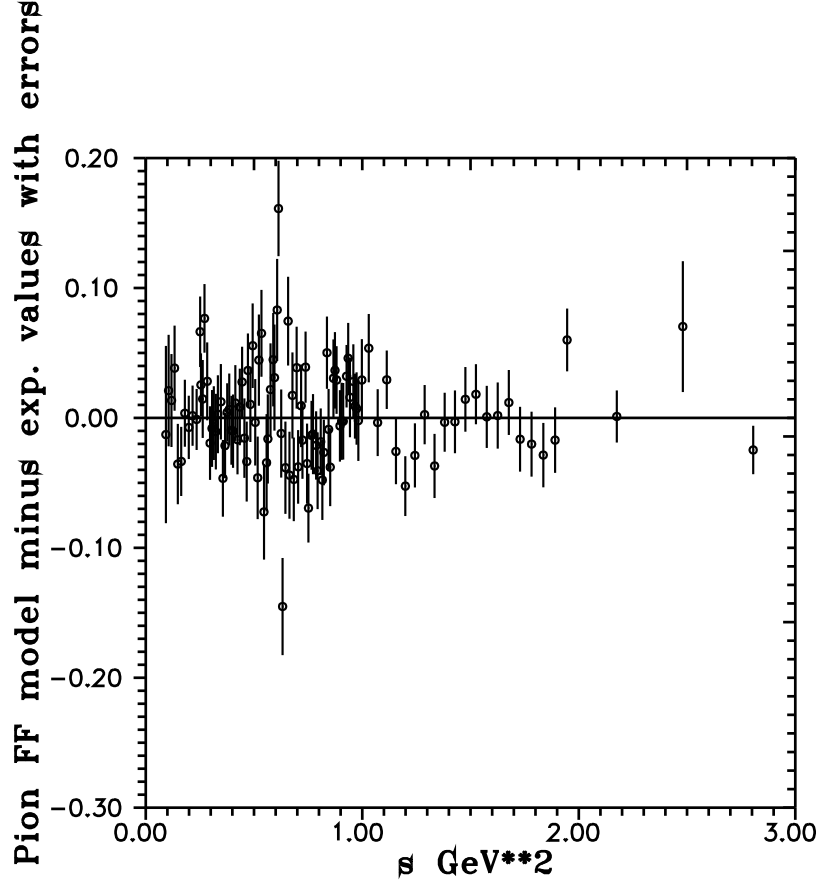


FIG. 11. Graphical demonstration of a subtraction of the full line data in Figure 10 from the pure EM form factor $|F_\pi^c(s)|$ data as given in Tables 2–4 reveal no damped oscillatory structures.

- [12] Baldini Ferroli, R.; Pacetti, S.; Zallo, A. No Sommerfeld resummation factor in $e^+e^- \rightarrow p\bar{p}$? *Eur. Phys. J. A* **2012**, *48*, 33. <https://doi.org/10.1140/epja/i2012-12033-6>.
- [13] Tomasi-Gustafsson, E.; Rekalo, M.P. Search for evidence of asymptotic regime of nucleon electromagnetic form-factors from a compared analysis in space- and time-like regions. *Phys. Lett. B* **2001**, *504*, 291–295. [https://doi.org/10.1016/S0370-2693\(01\)00312-4](https://doi.org/10.1016/S0370-2693(01)00312-4).
- [14] Dunning, J.R.; Chen, K.W.; Cone, A.A.; Hartwig, G.; Ramsey, N.F.; Walker, J.K.; Wilson, R. Quasi-Elastic Electron-Deuteron Scattering and Neutron Form Factors. *Phys. Rev.* **1966**, *141*, 1286–1297. <https://doi.org/10.1103/PhysRev.141.1286>.
- [15] Akhiezer, A.I.; Rekalo, M.P. Polarization phenomena in electron scattering by protons in the high energy region. *Sov. Phys. Dokl.* **1968**, *13*, 572.
- [16] Akhiezer, A.I.; Rekalo, M.P. Polarization effects in the scattering of leptons by hadrons. *Sov. J. Part. Nucl.* **1974**, *4*, 277.
- [17] Jones, M.K.; Aniol, K.A.; Baker, F.T.; Berthot, J.; Bertin, P.Y.; Bertozzi, W.; Besson, A.; Bimbot, L.; Boeglin, W.U.; Brash, E.J.; et al. G_{E_p}/G_{M_p} Ratio by Polarization Transfer in $\vec{e} p \rightarrow e \vec{p}$. *Phys. Rev. Lett.* **2000**, *84*, 1398–1402. <https://doi.org/10.1103/PhysRevLett.84.1398>.

- [18] Gayou, O.; Aniol, K.A.; Averett, T.; Benmokhtar, F.; Bertozzi, W.; Bimbot, L.; Brash, E.J.; Calarco, J.R.; Cavata, C.; Chai, Z.; et al. Measurement of G_{E_p}/G_{M_p} in $\vec{e} p \rightarrow e \vec{p}$ to $Q^2 = 5.6\text{GeV}^2$. *Phys. Rev. Lett.* **2002**, *88*, 092301. <https://doi.org/10.1103/PhysRevLett.88.092301>.
- [19] Punjabi, V.; Perdrisat, C.F.; Aniol, K.A.; Baker, F.T.; Berthot, J.; Bertin, P.Y.; Bertozzi, W.; Besson, A.; Bimbot, L.; Boeglin, W.U.; et al. Proton elastic form factor ratios to $Q^2 = 3.5\text{ GeV}^2$ by polarization transfer. *Phys. Rev. C* **2005**, *71*, 055202. <https://doi.org/10.1103/PhysRevC.71.055202>.
- [20] Zhan, X.; Allada, K.; Armstrong, D.S.; Arrington, J.; Bertozzi, W.; Boeglin, W.; Chen, J.-P.; Chirapatpimol, K.; Choi, S.; Chudakov, E.; et al. High-precision measurement of the proton elastic form factor ratio $\mu_p G_E/G_M$ at low Q^2 . *Phys. Lett. B* **2011**, *705*, 59–64. <https://doi.org/https://doi.org/10.1016/j.physletb.2011.10.002>.
- [21] Puckett, A.J.R.; Brash, E.J.; Jones, M.K.; Luo, W.; Meziane, M.; Pentchev, L.; Perdrisat, C.F.; Punjabi, V.; Wesselmann, F.R.; Afanasev, A.; et al. Polarization transfer observables in elastic electron-proton scattering at $Q^2 = 2.5, 5.2, 6.8$, and 8.5GeV^2 . *Phys. Rev. C* **2017**, *96*, 055203. <https://doi.org/10.1103/PhysRevC.96.055203>.
- [22] Bianconi, A.; Tomasi-Gustafsson, E. Periodic interference structures in the timelike proton form factor. *Phys. Rev. Lett.* **2015**, *114*, 232301. <https://doi.org/10.1103/PhysRevLett.114.232301>.
- [23] Ablikim, M. Oscillating features in the electromagnetic structure of the neutron. *Nat. Phys.* **2021**, *17*, 1200–1204. <https://doi.org/10.1038/s41567-021-01345-6>.
- [24] Bianconi, A.; Tomasi-Gustafsson, E. Phenomenological analysis of near-threshold periodic modulations of the proton timelike form factor. *Phys. Rev. C* **2016**, *93*, 035201. <https://doi.org/10.1103/PhysRevC.93.035201>.
- [25] Tomasi-Gustafsson, E.; Pacetti, S. Interpretation of recent form factor data in terms of an advanced representation of baryons in space and time. *Phys. Rev. C* **2022**, *106*, 035203. <https://doi.org/10.1103/PhysRevC.106.035203>.
- [26] Lorenz, I.T.; Hammer, H.W.; Meißner, U.G. New structures in the proton-antiproton system. *Phys. Rev. D* **2015**, *92*, 034018. <https://doi.org/10.1103/PhysRevD.92.034018>.
- [27] Lees, J.P.; Poireau, V.; Tisserand, V.; Tico, J.G.; Grauges, E.; Palano, A.; Eigen, G.; Stugu, B.; Brown, D.N.; Kerth, L.T.; et al. Precise Measurement of the $e^+e^- \rightarrow \pi^+\pi^-(\gamma)$ Cross Section with the Initial-State Radiation Method at BABAR. *Phys. Rev.* **2012**, *D86*, 032013. <https://doi.org/10.1103/PhysRevD.86.032013>.
- [28] Xiao, T.; Dobbs, S.; Tomaradze, A.; Seth, K.K.; Bonvicini, G. Precision measurement of the hadronic contribution to the muon anomalous magnetic moment. *Phys. Rev. D* **2018**, *97*, 032012. <https://doi.org/10.1103/PhysRevD.97.032012>.
- [29] Ablikim, M.; Achasov, M.N.; Adlarson, P.; Ahmed, S.; Albrecht, M.; Aliberti, R.; Amoroso, A.; An, Q.; Bai, X.H.; Bai, Y.; et al. Corrigendum to “Measurement of the $e^+e^- \rightarrow \pi^+\pi^-$ cross section between 600 and 900 MeV using initial state radiation” [Phys. Lett. B 753 (2016) 629–638]. *Phys. Lett. B* **2021**, *812*, 135982. <https://doi.org/https://doi.org/10.1016/j.physletb.2020.135982>.

- [30] Dubnicka, S.; Dubnickova, A. Analyticity in a phenomenology of electro-weak structure of hadrons. *Acta Phys. Slov.* **2010**, *60*, 1–153.
- [31] Particle Data Group; Zyla, P.A.; Barnett, R.M.; Beringer, J.; Dahl, O.; Dwyer, D.A.; Groom, D.E.; Lin, C.-J.; Lugovsky, K.S.; Pianori, E.; et al. Review of Particle Physics. *PTEP* **2020**, *2020*, 083C01. <https://doi.org/10.1093/ptep/ptaa104>.
- [32] Biagini, M.E.; Dubnicka, S.; Etim, E.; Kolar, P. Phenomenological evidence for a third radial excitation of $\rho(770)$. *Il Nuovo Cimento D* **1991**, *104*, 363–370. <https://doi.org/10.1007/BF02799144>.
- [33] Garcia-Martin, R.; Kaminski, R.; Pelaez, J.R.; Ruiz de Elvira, J.; Yndurain, F.J. The Pion-pion scattering amplitude. IV: Improved analysis with once subtracted Roy-like equations up to 1100 MeV. *Phys. Rev.* **2011**, *D83*, 074004. <https://doi.org/10.1103/PhysRevD.83.074004>.
- [34] Bartoš, E.; Dubnička, S.; Liptaj, A.; Dubničková, A.Z.; Kamiński, R. What are the correct $\rho^0(770)$ meson mass and width values? *Phys. Rev.* **2017**, *D96*, 113004. <https://doi.org/10.1103/PhysRevD.96.113004>.